Cell Reports
Article

Cell PRESS
Open ACCESS

Higher-Order Looping and Nuclear Organization of *Tcra* Facilitate Targeted RAG Cleavage and Regulated Rearrangement in Recombination Centers

Julie Chaumeil,[1] Mariann Micsinai,[1,2,3,5] Panagiotis Ntziachristos,[1] Ludovic Deriano,[1,10] Joy M.-H. Wang,[1] Yanhong Ji,[6,11] Elphege P. Nora,[8] Matthew J. Rodesch,[9] Jeffrey A. Jeddeloh,[9] Iannis Aifantis,[1,4] Yuval Kluger,[5] David G. Schatz,[6,7] and Jane A. Skok[1,3,*]

[1]Department of Pathology
[2]NYU Center for Health Informatics and Bioinformatics
[3]NYU Cancer Institute
[4]Howard Hughes Medical Institute
New York University School of Medicine, New York, NY 10016, USA
[5]Department of Pathology and Yale Cancer Center
[6]Department of Immunobiology
[7]Howard Hughes Medical Institute
Yale University School of Medicine, New Haven, CT 06520, USA
[8]Institut Curie, CNRS UMR3215, INSERM U934, Paris 75005, France
[9]Roche Nimblegen, Inc., Madison, WI 53719, USA
[10]Present address: Lymphocyte Development and Oncogenesis Group, Immunology Department, Pasteur Institute, Paris 75015, France
[11]Present address: Department of Immunology and Microbiology, School of Medicine Xi'an Jiaotong University, Xi'an 710061, China
*Correspondence: jane.skok@med.nyu.edu
http://dx.doi.org/10.1016/j.celrep.2013.01.024

SUMMARY

V(D)J recombination is essential for generating a diverse array of B and T cell receptors that can recognize and combat foreign antigens. As with any recombination event, tight control is essential to prevent the occurrence of genetic anomalies that drive cellular transformation. One important aspect of regulation is directed targeting of the RAG recombinase. Indeed, RAG accumulates at the 3′ end of individual antigen receptor loci poised for rearrangement; however, it is not known whether focal binding is involved in regulating cleavage, and what mechanisms lead to enrichment of RAG in this region. Here, we show that monoallelic looping out of the 3′ end of the T cell receptor α (*Tcra*) locus, coupled with transcription and increased chromatin/nuclear accessibility, is linked to focal RAG binding and ATM-mediated regulation of monoallelic cleavage on looped-out 3′ regions. Our data identify higher-order loop formation as a key determinant of directed RAG targeting and the maintenance of genome stability.

INTRODUCTION

Epigenetic regulation of gene expression involves dynamic changes in transcription factor (TF) binding, chromatin packaging, and nuclear organization. In recent years, we have learned a great deal about the genome-wide binding patterns of TFs and chromatin marks that determine the "on" or "off" state of target genes in a given lineage and developmental stage. These data sets are beginning to be integrated with genome-wide chromosome conformation capture analyses to determine how binding patterns translate into changes in nuclear organization. The combined information from these experiments indicates that coregulated active and repressed genes contact each other in activator or repressor-enriched regions of the nucleus, respectively (Cheutin and Cavalli, 2012; Schoenfelder et al., 2010). Aggregation of coregulated genes in a population of cells implies the interaction of multiple different loci. However, individual chromosomes occupy discrete territories in interphase nuclei, and, bearing in mind these physical constraints, it is not clear how genes on different chromosomes meet up with each other in the nucleus to form hubs. In fact, live imaging studies indicate that chromosome territories move very little after mitosis; thus, unless chromosome territories are neighboring, gene interactions must rely on the mobility of individual loci, which are known to be more dynamic (Müller et al., 2010). Higher-order looping facilitates movement of genes away from their chromosome territories, and this is often correlated with open chromatin and an active transcriptional status, while silent genes are positioned more internally (Fraser and Bickmore, 2007; Heard and Bickmore, 2007; Kalhor et al., 2012; Splinter et al., 2011). However, while higher-order looping has been shown to facilitate stochastic interactions between genes on different chromosomes (Kalhor et al., 2012), we know little about whether higher-order looping contributes to coordinated regulation of genes in *trans*.

The antigen-receptor loci have afforded a rich model for studying the epigenetic mechanisms underlying regulation of programmed recombination in developing lymphocytes. It has

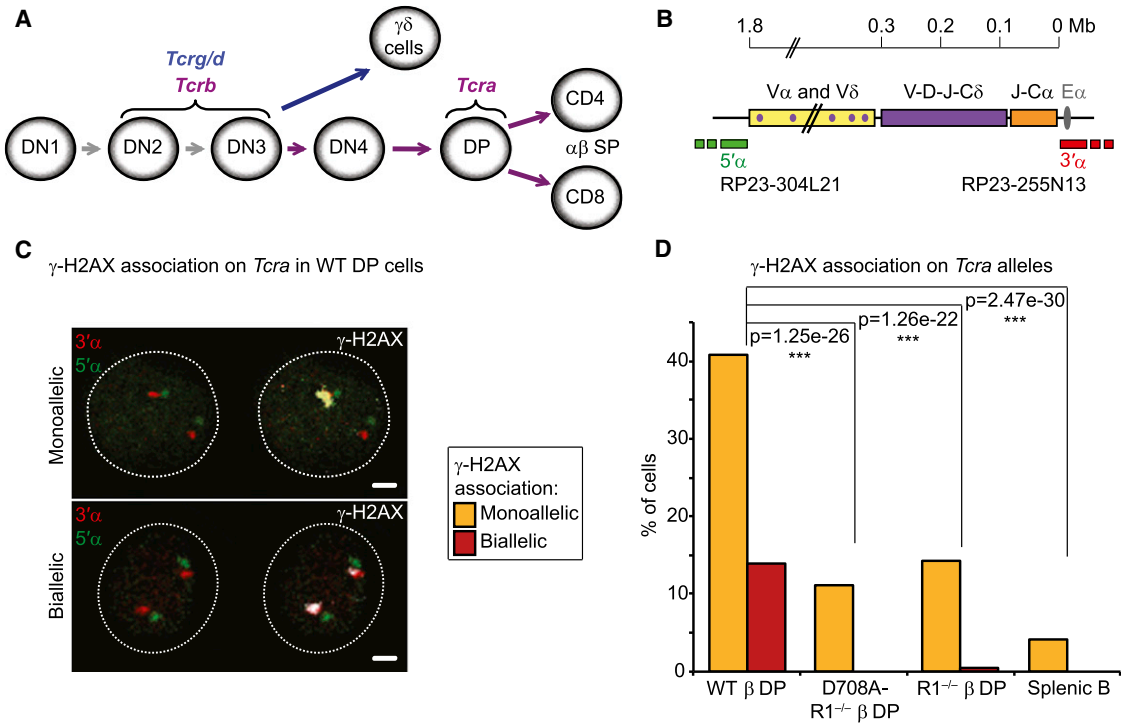

Figure 1. Recombination of *Tcra* Occurs on One Allele at a Time in DP Cells

(A) Recombination of the four *Tcr* loci is shown at different stages of T cell development.

(B) This scheme represents the *Tcra/d* locus. Probes for 3D-DNA FISH were generated from BACs hybridizing outside of the Vα segments (5′α, green) and of the Cα region (3′α, red).

(C) Confocal sections show examples of γ-H2AX association (in white) on *Tcra* alleles (3′α in red and 5′α in green) in WT DP cells: monoallelic association on the top panel and biallelic association with the two foci of different size and intensity, on the bottom panel. Scale bars = 1 μm.

(D) The frequency of γ-H2AX association on *Tcra* is shown for WT, RAG1 mutant DP cells, and splenic B cells.

The p values calculated using a two-tailed Fisher's exact test are shown as: ns, no significance ($p \geq 5.00e\text{-}2$); *, significant ($5.00e\text{-}2 > p \geq 1.00e\text{-}2$); **, very significant ($1.00e\text{-}2 > p \geq 1.00e\text{-}3$); ***, highly significant ($p < 1.00e\text{-}3$). Graphs and p values represent a combination of two independent and representative experiments (individual data sets and full statistical analyses in Table S1).

See also Figure S1.

been shown that intralocus loop formation (locus contraction), changes in chromatin landscape, and dynamic association of antigen-receptor loci with repressive pericentromeric heterochromatin (PCH) contribute (Chaumeil and Skok, 2012; Hewitt et al., 2010). However, we do not know how higher-order nuclear organization of antigen receptor loci is integrated with these various aspects of regulation and what role it plays in controlling this complex process in individual cells. This is particularly pertinent in light of recent data showing that the lymphoid-specific recombinase proteins, RAG1 and RAG2, bind to active chromatin and localize to the J segments at the 3′ end of each antigen receptor locus in rearranging cells (Ji et al., 2010). How focal RAG binding alters higher-order nuclear organization and the regulation of cleavage has not been investigated.

V(D)J recombination of *immunoglobulin* (*Ig*) and *T cell receptor* (*Tcr*) loci occurs in developing B and T cells, respectively. Tight control is exerted at multiple levels to ensure lineage and stage-specific rearrangement of variable (V), diversity (D), and joining (J) gene segments within the individual loci. Furthermore, recombination is regulated at the level of the individual allele (allelic exclusion) to ensure that each B and T cell expresses an antigen receptor with limited specificity. The RAG proteins recognize highly conserved recombination signal sequences (RSSs) bordering each V, D, and J gene segment (Helmink and Sleckman, 2012; Schatz and Ji, 2011). RAG binding mediates synapsis of a pair of compatible RSSs (that have conserved heptamer and nonamer sequences separated by a 12 and 23 bp space) prior to cleavage, and, following the introduction of double-strand breaks (DSBs), the recombinase secures the four broken ends in a postcleavage complex. Repair of these recombination intermediates occurs through the combined action of the DNA damage response pathway (which involves the factors ATM, γ-H2AX, 53BP1, and the MRN complex) as well as the ubiquitous nonhomologous end joining (NHEJ) machinery (Helmink and Sleckman, 2012; Puebla-Osorio and Zhu, 2008). This gives rise to a new antigen receptor gene and a signal joint, which is frequently excised during cell division.

Productive rearrangement of the different *Tcr* loci gives rise to two distinct T cell lineages: recombination of *Tcrg/Tcrd* and *Tcrb/Tcra* leads to γδ and αβ T cells, respectively (Figure 1A) (Ciofani and Zúñiga-Pflücker, 2010; Krangel, 2009). Rearrangement of the *Tcrg*, *Tcrd*, and *Tcrb* loci occurs early on in

development in $CD4^{-}CD8^{-}$ double-negative DN2/3 cells, while *Tcra* recombination occurs later at the double-positive (DP) stage (Livák et al., 1999). Because the *Tcrd* locus is embedded within the *Tcra* locus (Figure 1B), regulation of *Tcrd* and *Tcra* recombination is especially complex. Furthermore, the *Tcrd* and *Tcra* loci are not stringently subjected to allelic exclusion, and productively assembled genes are frequently biallelically expressed. Thus, recombination can occur on both alleles. Moreover, individual *Tcra* alleles typically undergo numerous recombination events in each DP cell. Given the large number of recombination events that can occur during *Tcra* assembly, tight control at the DP cell stage is particularly important. Here, we have investigated the role of transcription, higher-order looping, and nuclear organization in regulating these processes to safeguard genome stability.

RESULTS

Recombination of *Tcra* Occurs on One Allele at a Time in DP Cells

As the *Tcra* locus is not subject to allelic exclusion, we first asked whether both *Tcra* alleles are targeted for recombination at the same time. For this, we examined RAG-mediated cleavage of *Tcra* in individual DP cells by 3D immuno-DNA fluorescence in situ hybridization (FISH), using two differentially labeled bacterial artificial chromosome (BAC) probes that hybridize to the 3′α and 5′α ends of the locus (which in the germline form are 1.8 Mb apart) (Skok et al., 2007) in combination with an antibody that detects the phosphorylated form of the histone variant H2AX (γ-H2AX) as a readout for DSBs (Chen et al., 2000; Rogakou et al., 1998) (Figures 1B and 1C). For these studies, we sorted DP cells from RAG1-deficient and control wild-type mice, known as $R1^{-/-}$ β and WT β, respectively. Both mice carry a functionally rearranged *Tcrb* transgene (β) that allows T cell development to proceed to the DP stage in the absence of *Tcrb* rearrangement. As a complementary control, we also included DP cells from D708A-$R1^{-/-}$ β mice, which, in addition to the *Tcrb* transgene, carry another transgene expressing a catalytically inactive version of the RAG1 protein that has a D708A active site substitution preventing DNA cleavage without impairing binding and synapsis of RSSs by the RAG complex (Fugmann et al., 2000; Kim et al., 1999; Landree et al., 1999).

As expected, we found that γ-H2AX was associated with *Tcra* at very low levels in control splenic B cells, while in WT or WT β DP cells, consistent with a previous study (Chen et al., 2000), foci of γ-H2AX were colocalized with one *Tcra* allele in around 40% of cells and with both alleles in around 14% of the cells (Figures 1C and 1D; Table S1). We noticed, however, that in more than 80% of WT DP cells harboring biallelic breaks, one γ-H2AX focus was substantially smaller in size and intensity than the other, even though the two DNA FISH signals were equivalent (see surface plots in Figure S1A). Furthermore, in RAG-deficient cells monoallelic γ-H2AX association on *Tcra* alleles occurred at a similar frequency as the biallelic breaks in WT cells (around 14%), with similar small and faint foci as those found on the second allele in WT cells (Figures 1D, S1A, and S1B). These data indicate that only the large γ-H2AX foci in WT cells are specific to RAG-mediated cleavage, whereas the small RAG-independent foci may result from other cellular processes such as transcription. Indeed, the difference between the level of γ-H2AX association on *Tcra* alleles in RAG-deficient and splenic B cells suggests that transcription could be a factor. Thus, despite the absence of allelic exclusion, RAG-mediated cleavage of *Tcra* occurs on one allele at a time in DP cells.

Monoallelic Higher-Order Looping out of the *Tcra* 3′ End Coincides with Monoallelic RAG-Mediated Cleavage

To investigate whether differential organization of *Tcra* alleles relative to their chromosome territories could be involved in asynchronous RAG cleavage on the two *Tcra* alleles, we performed 3D DNA FISH for *Tcra* combined with a chromosome 14 paint. For our analysis, we classified the location of *Tcra* relative to the chromosome territory into the following four categories: (1) outside: looping out of the bulk of the chromosome territory (defined here as higher-order loops), (2) outer edge: adjacent to the territory edge, (3) edge: spanning the territory edge, and (4) inside the territory (see Extended Experimental Procedures for details). Interestingly, we found that *Tcra* was more likely to adopt an external location and form large higher-order loops outside of the chromosome territory in the presence of WT or catalytically inactive RAG1 (Figures 2A and S2A; Table S2). In contrast, in splenic B cells where *Tcra* is transcriptionally inactive and RAG is not expressed, the alleles adopted a more internal location compared to RAG1 mutant DP cells, in which *Tcra* is active. Thus, consistent with previous published reports (for review, see Heard and Bickmore, 2007), transcription may be linked to looping out. Here, however, we have also uncovered an additional aspect of control: higher-order loop formation is dependent on *trans*-acting factors (in this case the RAG recombinase).

Analysis of looped-out alleles showed that the majority had a decondensed conformation (separation of >0.5 μm between the 3′α and 5′α ends), with the 3′α end positioned away from the chromosome 14 territory, while the 5′α end remained at the edge of the territory (Figures 2A and 2B, left; Table S2). (Additional points of discussion clarifying the differences between decondensation and decontraction can be found in Extended Results and Figure S2B.) Intriguingly, these higher-order loops were monoallelic more than 90% of the time (example in Figure 2A; Table S2). In a similar manner, γ-H2AX foci, which are predominantly monoallelic (Figure 1D), were mostly associated with decondensed *Tcra* alleles, and in the majority of cases these foci were located on the 3′α end alone and never on the 5′α end alone (Figures 2B, right, and S2C; Table S2). Furthermore, when breaks were detected in cells with one condensed and one decondensed allele, γ-H2AX foci were preferentially associated with the 3′ end of the latter (see example in Figure 2B).

To investigate higher-order looping in more depth, we designed a probe comprised of oligonucleotides that cover the entire *Tcra* locus with the exception of the most repetitive regions (see scheme below Figures 2C and 2D, Table S2 and Extended Experimental Procedures for details). (The use of complex oligonucleotide-based probes for FISH analysis was first described by Boyle et al., 2011.) With this probe, we could also detect deleted signal ends (a by-product of recombination) that were separated from the rest of the locus that was marked by the presence of the 3′α BAC (see asterisks in Figures 2C and 2D).

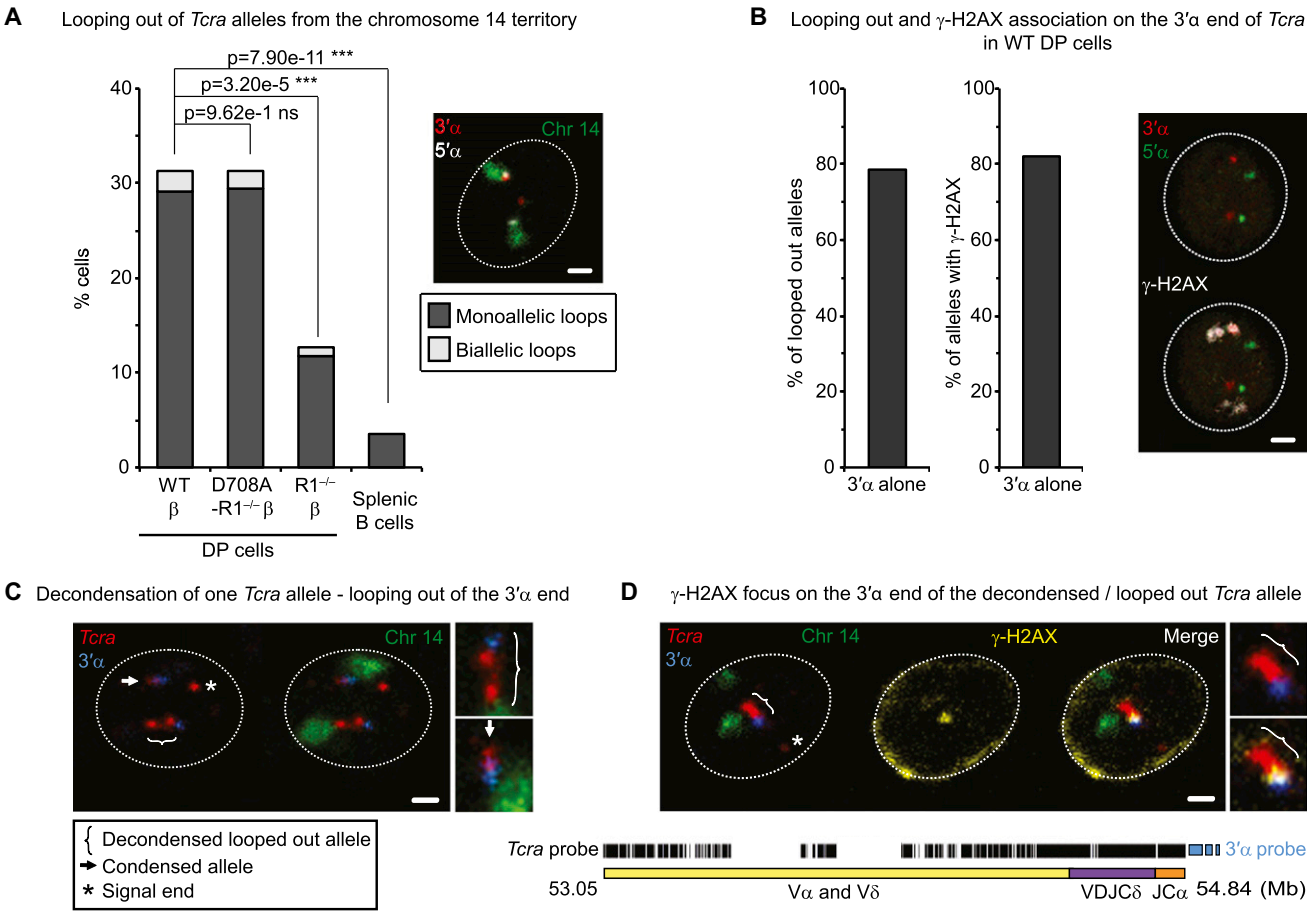

Figure 2. Monoallelic Higher-Order Looping of the 3′ End of *Tcra* Coincides with Monoallelic RAG-Mediated Cleavage

(A) Frequency of looping out of *Tcra* alleles from their chromosome 14 territories in WT, RAG1 mutant DP cells, and splenic B cells is shown. The p values were calculated using a two-tailed Fisher's exact test. Confocal section shows an example of monoallelic looping out of a decondensed *Tcra* allele: the 3′α end (red) loops out, while the 5′α (white) end remains inside of the chromosome 14 territory (green). Scale bar = 1 μm.

(B) Proportion of looped-out alleles (left) and alleles associated with γ-H2AX (right) that involve only the 3′α end of *Tcra* is shown. Confocal sections show an example of γ-H2AX association (white) on the 3′α end (red) of the decondensed *Tcra* allele (5′α in green). Scale bar = 1 μm.

(C and D) Confocal examples of monoallelic higher-order looping and decondensation of *Tcra* (C), correlated with γ-H2AX foci on the looped-out 3′α end (D), are shown. The scheme of the mix of oligonucleotide probes for the entire *Tcra/d* locus is shown below. *Tcra* is shown in red, 3′α in blue, chromosome 14 paint in green, and γ-H2AX in yellow. Scale bars = 1 μm.

See also Figure S2 and Table S2 for details and full statistical analyses.

(For additional points of discussion about signal ends, see Extended Results.) The combined use of this *Tcra* probe with the 3′α probe and the chromosome 14 paint showed that indeed looped-out alleles had a more elongated, decondensed conformation (with the 3′ region being the most external) compared to alleles that remained associated with the chromosome 14 territory (Figure 2C). Furthermore, immuno-DNA FISH confirmed that γ-H2AX foci were predominantly associated with the 3′ end of the looped-out decondensed alleles (Figure 2D).

Taken together, our data indicate that monoallelic higher-order looping of *Tcra*, which separates the 3′ end from the chromosome territory, occurs in a RAG-dependent, cleavage-independent manner, indicating that this change in nuclear conformation occurs prior to the introduction of a break. Moreover, the link between monoallelic looping out of the 3′α end of *Tcra* and monoallelic association of γ-H2AX foci in this 3′α region suggests that these changes in nuclear organization could participate in the regulation of recombination.

Looping out of the 3′ End of *Tcra* Is Linked to Transcription, Increased Accessibility, and Monoallelic Cleavage

To further understand the mechanism underlying the formation of monoallelic higher-order loop formation, we performed sequential RNA/DNA FISH, with nascent RNA detected by the large *Tcra* probe (see Figures 2C and 2D) followed by DNA FISH with the 3′α probe and the chromosome 14 paint in WT DP cells. Briefly, RNA FISH was imaged by confocal microscopy, and coordinates of the fields of nuclei were recorded in order to track the nuclei after the subsequent DNA FISH (see the sequential RNA/DNA FISH section of Extended Experimental Procedures for details). RNA signals were detected on both

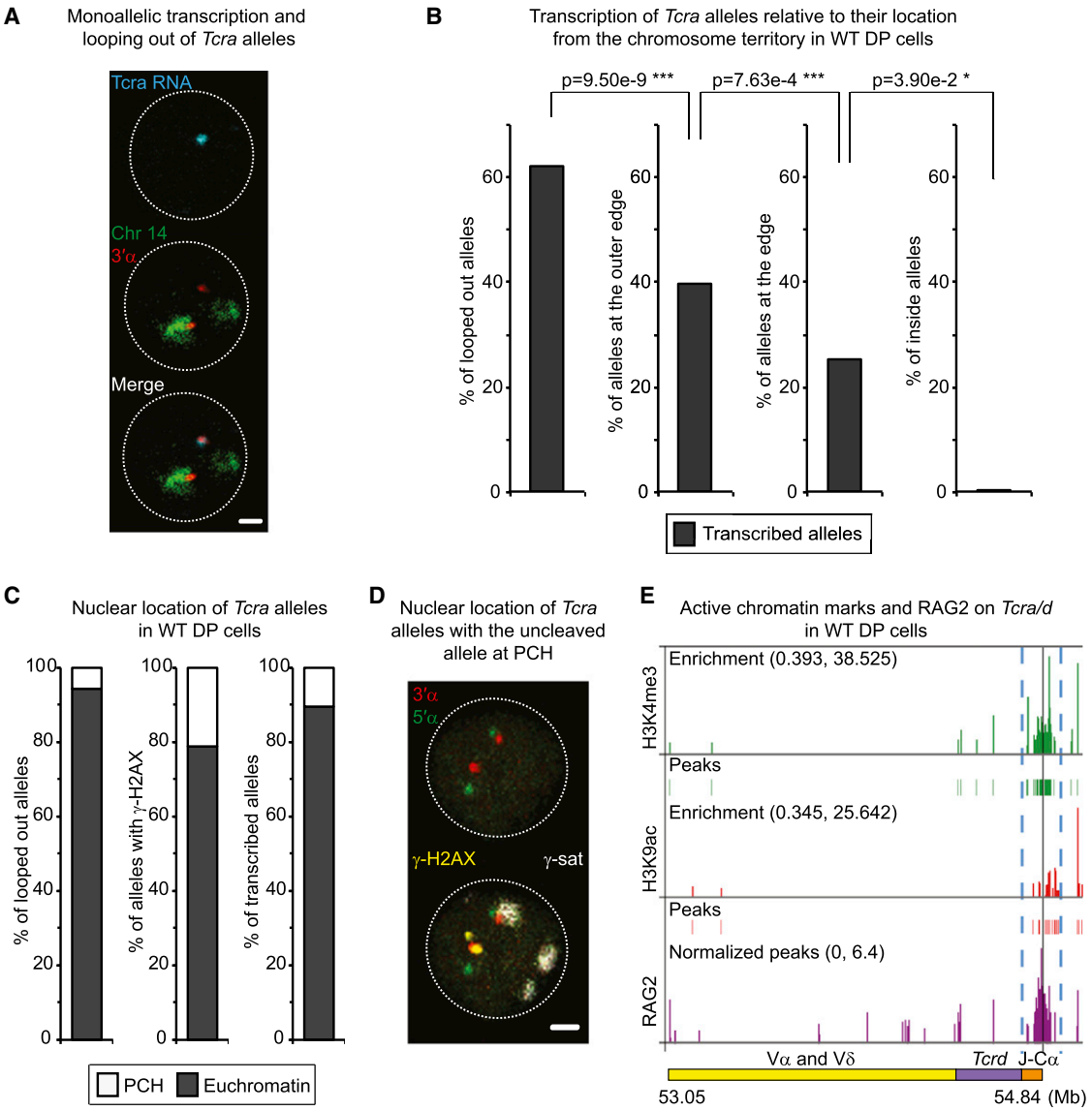

Figure 3. Looping Out of the 3′ End of *Tcra* Is Linked to Transcription, Increased Accessibility, and Monoallelic Cleavage

(A) Confocal example shows monoallelic transcription of looped-out *Tcra* allele. Merge was created subsequently based on the DAPI signals of the RNA FISH and DNA FISH images. *Tcra* nascent transcript is shown in blue, 3′α in red, chromosome 14 paint in green. Scale bar = 1 μm.

(B) Percentage of *Tcra* alleles located outside (loops), at the outer edge, at the edge, or inside the chromosome 14 territory, which are transcribed in WT DP cells, is shown. The p values were calculated using a two-tailed Fisher's exact test.

(C) Nuclear location of looped-out alleles (left), alleles associated with γ-H2AX (middle), and transcribed alleles (right) within euchromatin or heterochromatin (PCH) are shown.

(D) Confocal sections show an example of the uncleaved *Tcra* allele (no γ-H2AX) being at PCH, while the γ-H2AX-associated one remains in euchromatin. 3′α is shown in red, 5′α in green, γ-H2AX in yellow, and γ-satellite (PCH) in white. Scale bar = 1 μm.

(E) Alignment of ChIP-seq data at the *Tcra* locus shows levels of enrichment and peaks of H3K4me3 (green) and H3K9ac (red), as well as RAG2 binding (purple) (Ji et al., 2010). Blue dashed lines highlight the focal enrichment in active marks and RAG2 in the *Tcra* 3′α region.

See also Table S3 for details and full statistical analyses.

alleles in 26.3% of cells and on one allele in 30% of cells (in total 56% of cells had RNA signals) (Table S3). It is of note that, although the large *Tcra* probe was used for this analysis, RNA signals were predominantly only found associated with the 3′ end of the locus (see example in Figure 3A). This is likely due to limitations in detection of transcription below a certain level using this RNA FISH assay. Interestingly, transcription was correlated with the formation of higher-order loops: more looped-out *Tcra* alleles were transcribed compared to alleles that were positioned at the outer edge or edge of the territory (Figure 3B; Table S3). Furthermore, no RNA signals were found on alleles that were located inside the chromosome territory.

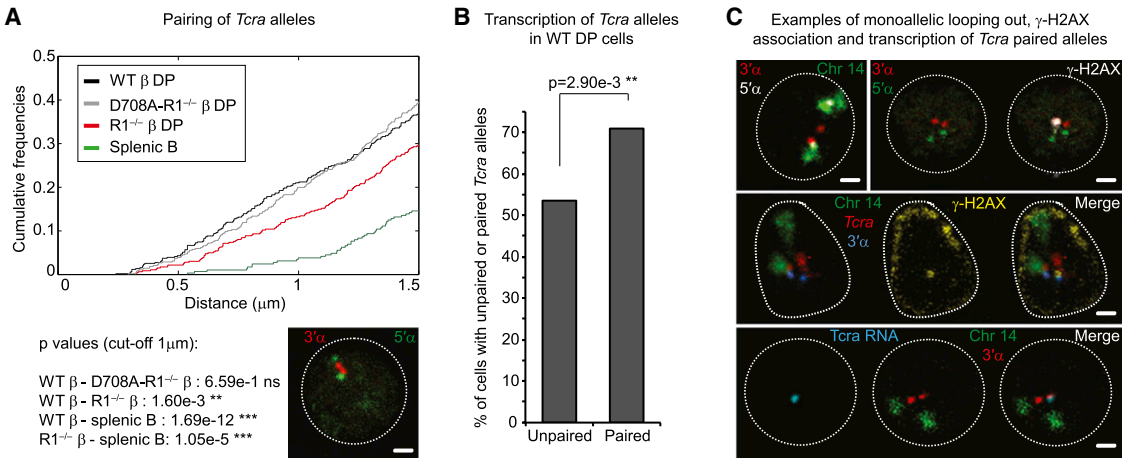

Figure 4. Homologous Pairing of *Tcra* Alleles Is Linked to Transcription, Increased Accessibility, and Monoallelic Cleavage

(A) Cumulative frequency curves of *Tcra* interallelic distances in WT, RAG1 mutant DP cells, and splenic B cells (cutoff at 1.5 μm; p values for a cutoff at 1 μm) are shown. A left shift indicates closer association. Confocal section shows paired *Tcra* alleles (3′α in red and 5′α in green). Scale bar = 1 μm.

(B) Frequency of transcription of unpaired and paired *Tcra* alleles assessed by RNA FISH-detecting nascent transcripts in WT DP cells is shown.

(C) Confocal sections show examples of monoallelic decondensation, looping out, association with γ-H2AX, and transcription in *Tcra* pairs in WT DP cells. Top left: 3′α in red, 5′α in white, and chromosome 14 paint in green. Top right: 3′α in red, 5′α in green, and γ-H2AX in white. Middle: *Tcra* in red, 3′α in blue, chromosome 14 paint in green, and γ-H2AX in yellow. Bottom: *Tcra* nascent transcript in blue, 3′α in red, chromosome 14 paint in green. Scale bars = 1 μm.

All p values were calculated using a two-tailed Fisher's exact test. See also Figure S3 and Table S4 for details and full statistical analyses.

Taken together, our data show that the formation of higher-order monoallelic *Tcra* loops is dependent on the presence of RAG as well as correlated with transcription.

We next asked whether looping of the 3′ end of the locus is linked to changes in accessibility and enrichment of RAG, which preferentially binds regions of active chromatin (Ji et al., 2010; Liu et al., 2007; Matthews et al., 2007; Shimazaki et al., 2009). To determine this, we examined the position of alleles relative to euchromatin (active chromatin) or to PCH (repressive chromatin that can be detected with a γ-satellite probe; Brown et al., 1999). Our analyses indicate that the vast majority of alleles that were (1) looped out, (2) associated with γ-H2AX, or (3) transcribed were positioned in euchromatic regions (Figure 3C; Table S3). Importantly, in cells with monoallelic γ-H2AX, the cleaved allele remained euchromatic, while the other uncleaved allele was predominantly positioned at PCH (example in Figure 3D). Further, chromatin immunoprecipitation (ChIP)-seq analyses of histone modifications (histone H3 lysine 4 trimethylation [H3K4me3] and histone H3 lysine 9 acetylation [H3K9ac]) confirmed that the 3′ end of *Tcra* was enriched for these active marks (Figure 3E; Table S3). Moreover, these marks line up with RAG2 enrichment in DP cells (data obtained from Ji et al., 2010) (Figure 3E). Together, these data suggest that monoallelic looping out of the 3′ end of *Tcra* in euchromatic regions as well as increased accessibility (active chromatin marks coupled with transcription) are linked to focal RAG binding and monoallelic cleavage in this region.

Homologous Pairing of *Tcra* Alleles Is Linked to Transcription, Increased Accessibility, and Monoallelic Cleavage

During the course of our analyses, we discovered that looped-out alleles were often in close proximity to their partner homologs. Moreover, we recently showed that homologous pairing and regulated asynchronous cleavage of *Ig* homologs are linked to allelic exclusion in developing B cells (Hewitt et al., 2009). We thus looked at whether *Tcra* alleles associate with one another in cells undergoing recombination. Our analyses of WT DP and control splenic B cells indicate that *Tcra* alleles were preferentially associated in T lineage cells (Figures 4A and S3A; Table S4). Sliding Fisher's exact tests comparing *Tcra* interallelic distances in WT β and R1$^{-/-}$ β DP cells showed that the lowest p values were found for distances under 1 μm (Chaumeil et al., 2013). Thus, consistent with previous studies (Augui et al., 2007; Bacher et al., 2006; Hewitt et al., 2009), we defined homologous pairing when the two alleles were separated by less than 1 μm from each other (Figures 4A and S3A; see Extended Experimental Procedures for details). Within the DP subset, we found that the frequency of homologous *Tcra* pairing was higher in WT β (or WT) compared to RAG1-deficient cells; however, the presence of the D708A catalytically inactive RAG1 protein was able to restore association to WT levels (Figure 4A; Table S4). Thus, the elevated level of pairing of *Tcra* alleles in DP cells depends on the presence of RAG1 but not on RAG-mediated cleavage, suggesting that pairing occurs prior to cleavage. This is analogous to what we observed for pairing of *Ig* loci in B cells (Hewitt et al., 2009). However, it is likely that other factors are also involved because pairing occurs at a higher frequency in RAG1-deficient DP cells compared to splenic B cells (Figure 4A). Since *Tcra* is transcribed in DP cells but not in splenic B cells, it is possible that transcriptional activity, in addition to the presence of RAG, promotes pairing. Indeed, the proportion of RNA signals in cells with paired alleles was significantly increased compared to cells with unpaired alleles (Figure 4B; Table S4). Thus, as with higher-order loop formation, pairing of homologs is dependent on the presence of RAG as well as correlated with transcription.

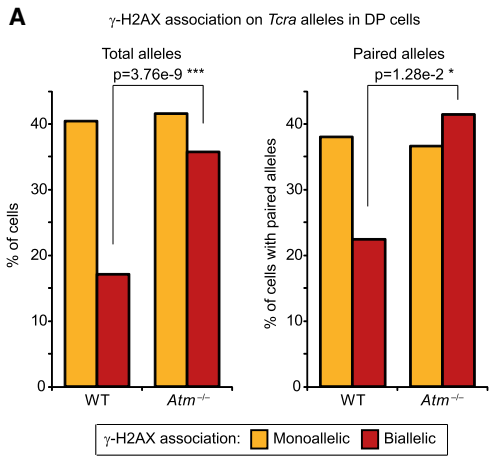

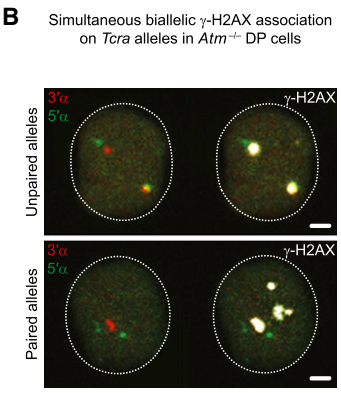

Figure 5. ATM Is Involved in Ensuring Monoallelic RAG-Mediated Cleavage on *Tcra* Alleles

(A) Frequency of γ-H2AX association on total (left) or paired (right) *Tcra* alleles in WT and *Atm*$^{-/-}$ DP cells is shown. The p values were calculated using a two-tailed Fisher's exact test.

(B) Confocal sections show examples of simultaneous biallelic γ-H2AX association on unpaired (top) and paired (bottom) *Tcra* alleles in *Atm*$^{-/-}$ DP cells. 3′α in red, 5′α in green, and γ-H2AX in white. Scale bars = 1 μm.

See also Figure S4 and Table S5 for details and full statistical analyses.

As for total alleles, we found that the formation of monoallelic higher-order loops involving the 3′ end of *Tcra*, monoallelic cleavage on the looped-out 3′ end, and association of the uncleaved allele with PCH also occurred on paired alleles (Figures 4C, S3B, and S3C; Table S4).

In summary, these data indicate that RAG1 enhances the propensity of one allele of *Tcra* to adopt a decondensed conformation, with the 3′α end of the locus looped away from its chromosome territory. Higher-order looping of the 3′α end coincides with transcription, focal RAG binding. and enrichment of active histone marks (Ji et al., 2010), as well as cleavage in this region, suggesting that these events are linked. We speculate that the formation of these higher-order loops could serve to bring RAG-enriched regions together in the nucleus, thereby increasing the concentration of RAG in localized recombination centers. The local concentration of RAG may also be a determinant of cleavage, in the sense that the more RAG that is present, the more likely the occurrence of a DSB. Furthermore, close proximity of RAG-enriched homologs provides a mechanism for *trans*-regulation of monoallelic cleavage.

ATM Is Involved in Ensuring Monoallelic RAG-Mediated Cleavage on *Tcra* Alleles

In developing B cells, RAG enhances homologous pairing of both *Igh* and *Igk* and repositioning of one allele to repressive PCH (Hewitt et al., 2009). Furthermore, the DNA-damage-sensing ATM is implicated in regulating monoallelic recombination in *trans* through repositioning of unrearranged *Ig* alleles to PCH: in the absence of ATM, both *Ig* alleles remain euchromatic, and there is a significant increase in biallelic breaks and translocations (Hewitt et al., 2009). Similarly, in DP cells we detected a significant increase in the frequency of γ-H2AX foci associated with both *Tcra* alleles in *Atm*$^{-/-}$ cells but no significant change in monoallelic γ-H2AX association (Figure 5A; Table S5). Moreover, in *Atm*$^{-/-}$ cells γ-H2AX formed two large foci of a similar size and intensity, which is in contrast to what we observed in WT cells with biallelic breaks (Figures 5B, S4A, and S4B).

One important aspect of ATM's regulation is to coordinate DSB repair with the progression of cell cycle through activation of proteins that regulate cell-cycle checkpoints, including Chk2 and p53 (Helmink and Sleckman, 2012). Thus, in the absence of ATM it is possible that unrepaired breaks could accrue as damaged alleles in dividing cells. However, since we only analyze intact alleles (see section below and Figures 6D and 6E for details on categories of damage) in DP cells and these are noncycling cells, the increase in biallelic breaks cannot be attributed to this aspect of control. Moreover, the increase in biallelic breaks is also not simply a result of a defect in repair, because in the absence of another DNA-damage-sensing factor, 53BP1, we did not observe the same phenotype. Rather, we found a significant increase in the frequency of monoallelic γ-H2AX foci associated with *Tcra*, suggesting that, in these cells, cleavage of the second allele cannot occur prior to repair of the first allele (Figure S4C; Table S5). These findings are in agreement with what we observed in *Artemis*$^{-/-}$ cells, which, due to an absence of this NHEJ factor, accumulate unrepaired RAG-mediated breaks: in the absence of Artemis, we observed breaks on only one allele, while in *Artemis*$^{-/-}$ *Atm*$^{-/-}$ cells breaks were found on both alleles (Hewitt et al., 2009). These data are consistent with the notion that RAG-mediated cleavage of *Tcra* is regulated to occur on one allele at a time through the action of ATM.

ATM-Mediated Suppression of Biallelic Cleavage and Preservation of Genome Integrity Involve Modulation of Nuclear Accessibility and Higher-Order Looping

To determine whether higher-order nuclear organization participates in coordinated ATM-mediated regulation of recombination on individual *Tcra* alleles, we simultaneously examined higher-order looping, homologous pairing, and association with PCH. Although ATM does not regulate association of *Tcra* homologs, we found that both paired and unpaired *Tcra* alleles were more frequently located in euchromatic regions of the nucleus in ATM-deficient versus control WT DP cells (Figures 6A, 6B, and S5A; Table S6). It is of note that in *53bp1*$^{-/-}$ DP cells we observed no significant change in homologous pairing or PCH association (Figures S5B and S5C; Table S6). Thus, repositioning of *Tcra* to PCH is dependent on ATM, and this function is not shared by all DNA-damage-sensing factors.

Importantly, we found that decreased association of *Tcra* with PCH in *Atm*$^{-/-}$ DP cells was linked to a significant increase in

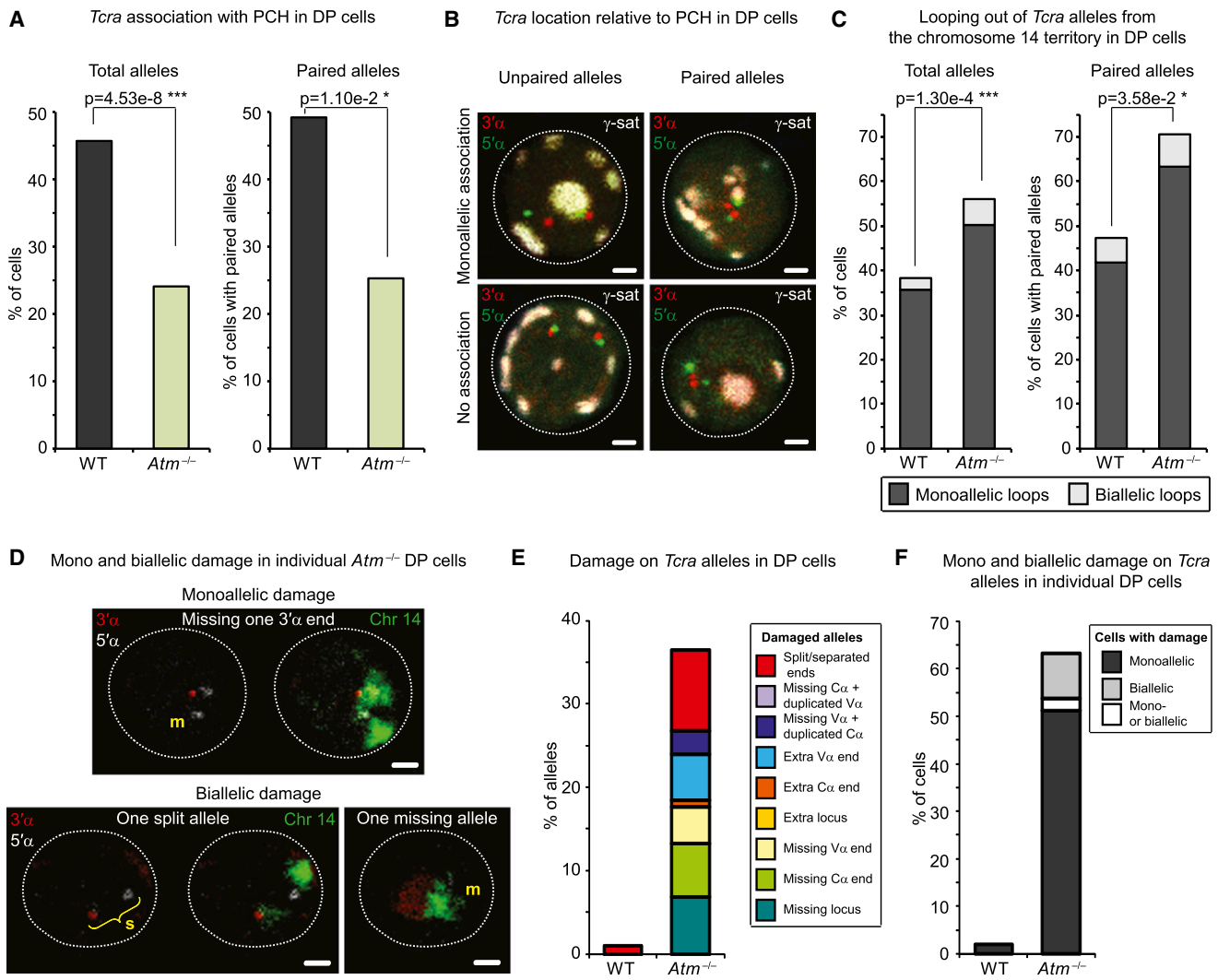

Figure 6. ATM-Mediated Suppression of Biallelic Cleavage and Preservation of Genome Integrity Involve Modulation of Nuclear Accessibility and Higher-Order Looping

(A) Frequency of PCH association of total (left) and paired (right) *Tcra* alleles in WT and *Atm*$^{-/-}$ DP cells is shown.

(B) Confocal sections show representative examples of unpaired (left) or paired (right) *Tcra* alleles associated with PCH (top) or not associated (bottom). 3′α is shown in red, 5′α in green, and γ-satellite (PCH) in white. Scale bars = 1 μm.

(C) Frequency of looping out of total (left) or paired (right) *Tcra* alleles from their chromosome 14 territories in WT and *Atm*$^{-/-}$ DP cells is shown.

(D) Confocal sections show examples of mono- and biallelic damage on *Tcra* alleles. 3′α is shown in red, 5′α in white, and chromosome 14 paint in green. m, missing end or locus; s, split locus. Scale bars = 1 μm.

(E and F) Frequency of damaged *Tcra* alleles (E) and frequency of cells with mono- or biallelic *Tcra* damage (F) in WT and *Atm*$^{-/-}$ DP cells are shown.

All p values were calculated using a two-tailed Fisher's exact test. See also Figure S5 and Table S6 for details and full statistical analyses.

higher-order looping out of paired and unpaired *Tcra* alleles (Figures 6C and S5D; Table S6). These data indicate that *trans*-regulation of monoallelic cleavage by ATM occurs by modulating nuclear accessibility of *Tcra* through changes in higher-order loop formation and PCH association. Recall that in cells with monoallelic γ-H2AX, the cleaved allele remained euchromatic while the uncleaved allele was predominantly positioned at PCH (Figure 3D). Thus, ATM, recruited to the site of a RAG-mediated break on one allele (directly or indirectly), acts in *trans* on the uncleaved allele, repositioning it to PCH and inhibiting loop formation.

To determine how ATM-mediated regulation of biallelic cleavage and changes in nuclear accessibility are linked with maintenance of genome stability, we next analyzed mono- and biallelic damage in *Atm*$^{-/-}$ interphase DP cells. For this, we performed a DNA FISH experiment using BAC probes that hybridize outside the 3′ and 5′ ends of *Tcra* (see scheme in Figure 1B) in combination with a chromosome 14 paint. Damage assessed included split alleles (>1.5 μm in between the two ends) and duplicated or missing signals (see examples in Figure 6D). Whereas only 1% of WT cells carried a *Tcra* allele with split ends, *Atm*$^{-/-}$ DP cells showed a whole range of damage on as

much as 37.2% of *Tcra* alleles (which represents 62.4% of cells carrying at least one damaged allele) (Figures 6D and 6E; Table S6). Importantly, in 9.6% of *Atm*$^{-/-}$ DP cells, both *Tcra* alleles were damaged in the same cell (Figures 6D and 6F; Table S6), which is consistent with previous analyses (Matei et al., 2007). In contrast, only monoallelic damage could be found in *53bp1*$^{-/-}$ DP cells, consistent with the increase in monoallelic γ-H2AX association (Figures S4C, S5E, and S5F; Table S6). In sum, ATM-mediated changes in nuclear organization (repositioning to PCH and higher-order looping) are linked with maintenance of genome stability. We suggest that these chromosomal movements could reduce accessibility to RAG proteins, preventing cleavage on the second allele, which could lead to genomic instability.

DISCUSSION

Although regulation of the *Tcra/d* locus is uniquely complicated, we have found that recombination occurs on only one allele at a time. As with *Ig* recombination, regulation of monoallelic cleavage occurs in *trans* through the action of ATM (Hewitt et al., 2009). To understand how recombination between different alleles is coordinated, we analyzed another aspect of nuclear organization: the formation of higher-order loops. Here, we show that higher-order monoallelic looping connects allelic interactions, transcription, active chromatin, nuclear accessibility, and focal RAG binding with monoallelic cleavage at the 3′ end of individual loci. These studies provide a plausible explanation for the mechanisms underlying directed monoallelic RAG targeting and regulated cleavage in localized recombination centers (Ji et al., 2010).

Previous studies have shown that dynamic movements of genes away from their chromosome territory are linked with their transcriptional status. For example, sequential looping out/decondensation of the *Hox* genes has been shown to be linked to expression (Chambeyron and Bickmore, 2004; Morey et al., 2009). Furthermore, X-linked genes are reorganized during X-chromosome inactivation, with internalization of repressed genes and looping out of escapees (Chaumeil et al., 2006). However, there have been no studies that connect gene interactions and regulation in *trans* with looping out of loci from their chromosome territories. Furthermore, higher-order looping was previously not known to play a role in recombination. Looping correlates with nuclear accessibility of the *Tcra* locus, as judged by transcription and its location in euchromatic regions of the nucleus. Moreover, in line with the notion that transcription can alter chromatin conformation and movement away from the chromosome territory, we found that the majority of looped-out *Tcra* alleles were decondensed, with the 3′ end separated from the 5′ end (which remained embedded in the territory), and RAG-mediated breaks were preferentially associated with the 3′ end of these alleles. Thus, we propose that transcription and focal binding of RAG at the 3′ end of the locus induce monoallelic looping/chromatin decondensation, which directs cleavage on one allele. Our data indicate that allelic differences in transcription could also contribute to the regulation of monoallelic cleavage, since DSBs are preferentially introduced on looped-out decondensed alleles, and the formation of the latter occur predominantly on transcribed alleles. Thus, allelic differences in transcription levels could determine which allele will be cleaved. Whether allelic differences are stochastic or the result of epigenetic differences linked to, for example, differences in chromatin packaging and replication timing (Farago et al., 2012; Goldmit et al., 2005; Mostoslavsky et al., 2001) remains to be determined.

Our data indicate that ATM mediates repositioning of the uncleaved allele to PCH, and movement to this repressive compartment is known to be accompanied by changes in chromatin and transcriptional repression (Su et al., 2004). Since active chromatin marks and transcription at the 3′ end of *Tcra* are both linked to higher-order looping out of the 3′ end of the locus, it is possible that inhibition of looping occurs on the uncleaved pericentric allele to prevent the introduction of further breaks in *trans*. This notion is supported by our finding that the vast majority of transcribed alleles were positioned in euchromatic regions. However, we do not conclude that repositioning to PCH is accompanied by complete transcriptional silencing on *Tcra* as it is likely our RNA FISH assay can only detect transcription occurring above a certain level. Thus, transcription could continue on repositioned loci, albeit at a reduced level (perhaps across a localized region) that could have an impact on higher-order loop formation. In addition, since we know that ATM-dependent chromatin changes silence transcription in *cis* to DNA double-strand breaks (Shanbhag et al., 2010), we cannot exclude that inhibition of looping out could also occur on the cleaved allele.

The experiments we have performed here provide additional insight into ATM-mediated regulation of RAG cleavage in *trans*. We know from our previous work that ATM (recruited to the site of a monoallelic *Ig* break) helps reposition uncleaved alleles to repressive pericentromeric heterochromatin (Hewitt et al., 2009). Here, we now show that ATM also functions to reduce accessibility by inhibiting higher-order loop formation. These changes in location and conformation correlate with inhibition of cleavage on the second allele. The temporal regulation of higher-order looping and PCH association are likely to be controlled by signaling pathways that have an impact on accessibility and transcription. Rapid release of alleles from heterochromatic regions and externalization from the territory could kick-start another round of recombination.

Our studies indicate that RAG-mediated looping away from the territory facilitates RAG-mediated interactions with homologous antigen receptor alleles, providing a mechanism for regulation of cleavage in *trans*. However, the changes in cleavage and accessibility that we observe on paired alleles are always mirrored at the level of the overall population, so we cannot rule out that regulation in *trans* is equally effective whether alleles are associated or separated, as shown in the two versions of the model (Figure S6). Nonetheless, we favor the first version in which ATM regulates nuclear accessibility and RAG-mediated cleavage of genes in the neighborhood of a DNA break (Figure S6). We propose that homologous alleles come together in localized recombination centers for coordinated regulation of RAG cleavage. Separation of alleles could occur during the repair phase of the break, which would account for the equivalent frequency of γ-H2AX association on paired and unpaired

alleles. Of course, in the absence of live-cell imaging studies that trace the dynamics of cleavage and repair at these loci, this is impossible to prove. Nonetheless, it is clear that closely associated uncleaved alleles will have immediate access to a high concentration of activated ATM and its downstream targets that accumulate at the site of the RAG break. Either way though, whether the mode of *trans*-regulation occurs on paired or unpaired alleles it is apparent that an ATM-mediated negative feedback loop provides a mechanism for limiting the number of RAG-mediated breaks that are introduced on antigen receptor alleles in each cell. Furthermore, this mode of regulation is linked to maintenance of genome stability in ATM-deficient mice (Callén et al., 2007; Deriano et al., 2011; Liyanage et al., 2000; Zha et al., 2010) and ataxia telangiectasia (AT) patients (Kobayashi et al., 1991).

Interestingly, our model for ATM-mediated feedback control of RAG cleavage at the site of a recombination break is remarkably similar to what has recently been proposed for ATM-mediated feedback regulation of recombination in meiosis (Lange et al., 2011). Activation of ATM by DSBs triggers a negative feedback loop that leads to the inhibition of closely associated SPO11-mediated DSB formation. In this context, it has also been proposed that feedback control operates at a local level to halt the introduction of further DSBs. Our data indicate that different programmed DNA recombination events share common regulatory mechanisms. As in meiosis, feedback control during V(D)J recombination could also be important for inhibiting further RAG cleavage in *cis* after the initial breaks are introduced. These studies provide further insight into the mechanisms underlying the regulation of recombination and the phenotype of the AT disease.

EXPERIMENTAL PROCEDURES

Mouse Strains

Appropriate wild-type mice (C57BL/6 CBA, 129, or WT β) or littermates were used as control mice for the mutant phenotypes. WT, *Rag1*$^{-/-}$ and *Rag1*$^{-/-}$-*Rag1*^{D708A} mice carrying a functionally rearranged *Tcrb* transgene (WT β, R1$^{-/-}$ β and D708A-R1$^{-/-}$ β) were provided by Yanhong Ji and David Schatz. The *Atm*$^{-/-}$ mice generated through the interbreeding of 129SvEv *Atm*$^{+/-}$ mice were given by Craig Bassing, Ludovic Deriano, and David Roth and genotyped as described (Barlow et al., 1996). The *53BP1*$^{-/-}$ mice were provided by Davide Robbiani and Michel Nussenzweig (Ward et al., 2003). Animal care was approved by the Institutional Animal Care and Use Committee. Protocol number is 120315-01 (NYU School of Medicine).

T Cell Flow Cytometry Sorting

Flow cytometry cell sorting was performed on a MoFlo or Reflection sorter. Antibodies were as follows: Thy1.2 PE-Cy7 (CD90.2, clone 53-2.1, eBioscience, 1:1,000 dilution), TCR-β APC-eFluor780 (clone H57-597, eBioscience, 1:500 dilution), CD4 APC (L3T4, RM4-5, BD Biosciences, 1:500 dilution), CD8a FITC (clone 53-6.7, BD Biosciences, 1:500 dilution), and CD25 PE (PC61, BD Biosciences, 1:500 dilution). Sorting was done as Thy1.2^{+}/TCRβ^{int}/CD4^{+}/CD8^{+} for DP cells and as Thy1.2^{+}/TCRβ^{lo}/CD4^{-}/CD8^{-}/CD25^{+} for DN2/3 cells.

Splenic B Cell Purification

B cells were purified from spleens of 6- to 10-week-old mice. Cells were suspended to 10^8 cells per 500 μl and labeled with magnetic microbeads coupled to anti-CD43 (Miltenyi Biotech, Auburn, CA) to remove T cells and macrophages. Cells were passed over a LS+ column following the manufacturer's instructions, and flowthrough B cells (CD43^{-}) were collected.

Probes for 3D DNA FISH

For details, see Supplemental Information.

3D DNA FISH and Immuno-FISH

3D-DNA FISH and combined DNA FISH immunofluorescence for γ-H2AX (immuno-FISH) were carried out on T or splenic B cells adhered to poly-L-lysine-coated coverslips or slides as previously described (Chaumeil et al., 2013). DNA FISH and immuno-FISH combined with the chromosome 14 paint were carried out as above except that the cells were denatured in 50% formamide/2× SSC (pH 7–7.4) for 30 min at 80°C before overnight hybridization, and the three washes were performed in 50% formamide/2× SSC (pH 7–7.4) and three times in 2× SSC at 37°C. For details, see Supplemental Information.

Sequential RNA/DNA FISH

Sequential RNA/DNA FISH was performed as previously described (Chaumeil et al., 2008). For details, see Supplemental Information.

Confocal Microscopy and Analysis

For details, see Supplemental Information.

Statistical Analysis

For details, see Supplemental Information.

ChIP-seq

Crosslinking of cells, preparation of mononucleosomes-containing chromatin, chromatin immunoprecipitation, and ChIP-Seq library preparation and sequencing were carried out as previously described using H3K9ac (Abcam) and H3K4me3 (Active Motif) antibodies (Ntziachristos et al., 2012). See Supplemental Information for details on ChIP-seq alignment and ChIP-seq analysis.

4C-seq

Splenic B cells (1 × 10^7) were processed as previously described (Simonis et al., 2006). Gene-specific PCR primers for *the Tcra* Eα enhancer bait were HindIII AGACAGACCCTGCGAAGCTT and DpnII TAAGACTGGACCCACAG AAC. The Illumina-specified adapters for Illumina GAIIx sequencing were included at the 5′ end of each primer. The 4C library was sequenced on an Illumina GAIIx single-read 72-cycle run. For details on analysis, see the Supplemental Information.

SUPPLEMENTAL INFORMATION

Supplemental Information includes Extended Results, Extended Experimental Procedures, six figures, and six tables and can be found with this article online at http://dx.doi.org/10.1016/j.celrep.2013.01.024.

LICENSING INFORMATION

ACKNOWLEDGMENTS

The authors thank M. Nussenzweig and D. Robbiani for providing the *53bp1*$^{-/-}$ mice, and C. Bassing, D. Roth, and L. Deriano for providing the *Atm*$^{-/-}$ mice. We would like to thank Jeanne Allinne, Susannah Hewitt, Pedro Rocha, Thomas Trimarchi, and MacLean Sellars for their help with 4C-seq experiments; Fabio Parisi and Francesco Strino for their help with statistical analyses; and members of the Skok lab for discussions and comments on the study. This work is supported by the National Institute of Health: R01GM086852 (to J.A.S.), R37AI32524 (to D.G.S.), RO1CA133379, RO1CA105129, RO1CA149655, and RO1GM088847 (to I.A.). J.A.S. is a Leukemia & Lymphoma Society (LLS) scholar. J.C. is an Irvington Institute

Fellow of the Cancer Research Institute. M.M. was supported by an NSF IGERT 0333389. L.D. was an LLS Fellow. E.P.N. was supported by the French Ministry of Research and the Association pour la Recherche sur le Cancer (France). I.A. is also supported by the Leukemia & Lymphoma Society (TRP grant), The V Foundation for Cancer Research, and the Dana Foundation. D.G.S. is an Investigator, and I.A. is an Early Career Scientist of the Howard Hughes Medical Institute. The authors from Roche NimbleGen, Inc. (M.J.R. and J.A.J.) recognize a competing interest in this publication as employees of the company.

Received: November 26, 2012
Revised: January 1, 2013
Accepted: January 16, 2013
Published: February 14, 2013

REFERENCES

Augui, S., Filion, G.J., Huart, S., Nora, E., Guggiari, M., Maresca, M., Stewart, A.F., and Heard, E. (2007). Sensing X chromosome pairs before X inactivation via a novel X-pairing region of the Xic. Science *318*, 1632–1636.

Bacher, C.P., Guggiari, M., Brors, B., Augui, S., Clerc, P., Avner, P., Eils, R., and Heard, E. (2006). Transient colocalization of X-inactivation centres accompanies the initiation of X inactivation. Nat. Cell Biol. *8*, 293–299.

Barlow, C., Hirotsune, S., Paylor, R., Liyanage, M., Eckhaus, M., Collins, F., Shiloh, Y., Crawley, J.N., Ried, T., Tagle, D., and Wynshaw-Boris, A. (1996). Atm-deficient mice: a paradigm of ataxia telangiectasia. Cell *86*, 159–171.

Boyle, S., Rodesch, M.J., Halvensleben, H.A., Jeddeloh, J.A., and Bickmore, W.A. (2011). Fluorescence in situ hybridization with high-complexity repeat-free oligonucleotide probes generated by massively parallel synthesis. Chromosome Res. *19*, 901–909.

Brown, K.E., Baxter, J., Graf, D., Merkenschlager, M., and Fisher, A.G. (1999). Dynamic repositioning of genes in the nucleus of lymphocytes preparing for cell division. Mol. Cell *3*, 207–217.

Callén, E., Jankovic, M., Difilippantonio, S., Daniel, J.A., Chen, H.T., Celeste, A., Pellegrini, M., McBride, K., Wangsa, D., Bredemeyer, A.L., et al. (2007). ATM prevents the persistence and propagation of chromosome breaks in lymphocytes. Cell *130*, 63–75.

Chambeyron, S., and Bickmore, W.A. (2004). Chromatin decondensation and nuclear reorganization of the HoxB locus upon induction of transcription. Genes Dev. *18*, 1119–1130.

Chaumeil, J., and Skok, J.A. (2012). The role of CTCF in regulating V(D)J recombination. Curr. Opin. Immunol. *24*, 153–159.

Chaumeil, J., Le Baccon, P., Wutz, A., and Heard, E. (2006). A novel role for Xist RNA in the formation of a repressive nuclear compartment into which genes are recruited when silenced. Genes Dev. *20*, 2223–2237.

Chaumeil, J., Augui, S., Chow, J.C., and Heard, E. (2008). Combined immunofluorescence, RNA fluorescent in situ hybridization, and DNA fluorescent in situ hybridization to study chromatin changes, transcriptional activity, nuclear organization, and X-chromosome inactivation. Methods Mol. Biol. *463*, 297–308.

Chaumeil, J., Micsinai, M., and Skok, J.A. (2013). Combined Immunofluorescence And DNA FISH on 3D-preserved Interphase Nuclei to Study Changes in 3D Nuclear Organization. J. Vis. Exp. *72*, e50087.

Chen, H.T., Bhandoola, A., Difilippantonio, M.J., Zhu, J., Brown, M.J., Tai, X., Rogakou, E.P., Brotz, T.M., Bonner, W.M., Ried, T., and Nussenzweig, A. (2000). Response to RAG-mediated VDJ cleavage by NBS1 and gamma-H2AX. Science *290*, 1962–1965.

Cheutin, T., and Cavalli, G. (2012). Progressive polycomb assembly on H3K27me3 compartments generates polycomb bodies with developmentally regulated motion. PLoS Genet. *8*, e1002465.

Ciofani, M., and Zúñiga-Pflücker, J.C. (2010). Determining γδ versus αβ T cell development. Nat. Rev. Immunol. *10*, 657–663.

Deriano, L., Chaumeil, J., Coussens, M., Multani, A., Chou, Y., Alekseyenko, A.V., Chang, S., Skok, J.A., and Roth, D.B. (2011). The RAG2 C terminus suppresses genomic instability and lymphomagenesis. Nature *471*, 119–123.

Farago, M., Rosenbluh, C., Tevlin, M., Fraenkel, S., Schlesinger, S., Masika, H., Gouzman, M., Teng, G., Schatz, D., Rais, Y., et al. (2012). Clonal allelic predetermination of immunoglobulin-κ rearrangement. Nature *490*, 561–565.

Fraser, P., and Bickmore, W. (2007). Nuclear organization of the genome and the potential for gene regulation. Nature *447*, 413–417.

Fugmann, S.D., Villey, I.J., Ptaszek, L.M., and Schatz, D.G. (2000). Identification of two catalytic residues in RAG1 that define a single active site within the RAG1/RAG2 protein complex. Mol. Cell *5*, 97–107.

Goldmit, M., Ji, Y., Skok, J., Roldan, E., Jung, S., Cedar, H., and Bergman, Y. (2005). Epigenetic ontogeny of the Igk locus during B cell development. Nat. Immunol. *6*, 198–203.

Heard, E., and Bickmore, W. (2007). The ins and outs of gene regulation and chromosome territory organisation. Curr. Opin. Cell Biol. *19*, 311–316.

Helmink, B.A., and Sleckman, B.P. (2012). The response to and repair of RAG-mediated DNA double-strand breaks. Annu. Rev. Immunol. *30*, 175–202.

Hewitt, S.L., Yin, B., Ji, Y., Chaumeil, J., Marszalek, K., Tenthorey, J., Salvagiotto, G., Steinel, N., Ramsey, L.B., Ghysdael, J., et al. (2009). RAG-1 and ATM coordinate monoallelic recombination and nuclear positioning of immunoglobulin loci. Nat. Immunol. *10*, 655–664.

Hewitt, S.L., Chaumeil, J., and Skok, J.A. (2010). Chromosome dynamics and the regulation of V(D)J recombination. Immunol. Rev. *237*, 43–54.

Ji, Y., Resch, W., Corbett, E., Yamane, A., Casellas, R., and Schatz, D.G. (2010). The in vivo pattern of binding of RAG1 and RAG2 to antigen receptor loci. Cell *141*, 419–431.

Kalhor, R., Tjong, H., Jayathilaka, N., Alber, F., and Chen, L. (2012). Genome architectures revealed by tethered chromosome conformation capture and population-based modeling. Nat. Biotechnol. *30*, 90–98.

Kim, D.R., Dai, Y., Mundy, C.L., Yang, W., and Oettinger, M.A. (1999). Mutations of acidic residues in RAG1 define the active site of the V(D)J recombinase. Genes Dev. *13*, 3070–3080.

Kobayashi, Y., Tycko, B., Soreng, A.L., and Sklar, J. (1991). Transrearrangements between antigen receptor genes in normal human lymphoid tissues and in ataxia telangiectasia. J. Immunol. *147*, 3201–3209.

Krangel, M.S. (2009). Mechanics of T cell receptor gene rearrangement. Curr. Opin. Immunol. *21*, 133–139.

Landree, M.A., Wibbenmeyer, J.A., and Roth, D.B. (1999). Mutational analysis of RAG1 and RAG2 identifies three catalytic amino acids in RAG1 critical for both cleavage steps of V(D)J recombination. Genes Dev. *13*, 3059–3069.

Lange, J., Pan, J., Cole, F., Thelen, M.P., Jasin, M., and Keeney, S. (2011). ATM controls meiotic double-strand-break formation. Nature *479*, 237–240.

Liu, Y., Subrahmanyam, R., Chakraborty, T., Sen, R., and Desiderio, S. (2007). A plant homeodomain in RAG-2 that binds Hypermethylated lysine 4 of histone H3 is necessary for efficient antigen-receptor-gene rearrangement. Immunity *27*, 561–571.

Livák, F., Tourigny, M., Schatz, D.G., and Petrie, H.T. (1999). Characterization of TCR gene rearrangements during adult murine T cell development. J. Immunol. *162*, 2575–2580.

Liyanage, M., Weaver, Z., Barlow, C., Coleman, A., Pankratz, D.G., Anderson, S., Wynshaw-Boris, A., and Ried, T. (2000). Abnormal rearrangement within the alpha/delta T-cell receptor locus in lymphomas from Atm-deficient mice. Blood *96*, 1940–1946.

Matei, I.R., Gladdy, R.A., Nutter, L.M., Canty, A., Guidos, C.J., and Danska, J.S. (2007). ATM deficiency disrupts Tcra locus integrity and the maturation of CD4+CD8+ thymocytes. Blood *109*, 1887–1896.

Matthews, A.G., Kuo, A.J., Ramón-Maiques, S., Han, S., Champagne, K.S., Ivanov, D., Gallardo, M., Carney, D., Cheung, P., Ciccone, D.N., et al. (2007). RAG2 PHD finger couples histone H3 lysine 4 trimethylation with V(D)J recombination. Nature *450*, 1106–1110.

Morey, C., Kress, C., and Bickmore, W.A. (2009). Lack of bystander activation shows that localization exterior to chromosome territories is not sufficient to up-regulate gene expression. Genome Res. *19*, 1184–1194.

Mostoslavsky, R., Singh, N., Tenzen, T., Goldmit, M., Gabay, C., Elizur, S., Qi, P., Reubinoff, B.E., Chess, A., Cedar, H., and Bergman, Y. (2001). Asynchronous replication and allelic exclusion in the immune system. Nature *414*, 221–225.

Müller, I., Boyle, S., Singer, R.H., Bickmore, W.A., and Chubb, J.R. (2010). Stable morphology, but dynamic internal reorganisation, of interphase human chromosomes in living cells. PLoS ONE *5*, e11560.

Ntziachristos, P., Tsirigos, A., Van Vlierberghe, P., Nedjic, J., Trimarchi, T., Flaherty, M.S., Ferres-Marco, D., da Ros, V., Tang, Z., Siegle, J., et al. (2012). Genetic inactivation of the polycomb repressive complex 2 in T cell acute lymphoblastic leukemia. Nat. Med. *18*, 298–301.

Puebla-Osorio, N., and Zhu, C. (2008). DNA damage and repair during lymphoid development: antigen receptor diversity, genomic integrity and lymphomagenesis. Immunol. Res. *41*, 103–122.

Rogakou, E.P., Pilch, D.R., Orr, A.H., Ivanova, V.S., and Bonner, W.M. (1998). DNA double-stranded breaks induce histone H2AX phosphorylation on serine 139. J. Biol. Chem. *273*, 5858–5868.

Schatz, D.G., and Ji, Y. (2011). Recombination centres and the orchestration of V(D)J recombination. Nat. Rev. Immunol. *11*, 251–263.

Schoenfelder, S., Sexton, T., Chakalova, L., Cope, N.F., Horton, A., Andrews, S., Kurukuti, S., Mitchell, J.A., Umlauf, D., Dimitrova, D.S., et al. (2010). Preferential associations between co-regulated genes reveal a transcriptional interactome in erythroid cells. Nat. Genet. *42*, 53–61.

Shanbhag, N.M., Rafalska-Metcalf, I.U., Balane-Bolivar, C., Janicki, S.M., and Greenberg, R.A. (2010). ATM-dependent chromatin changes silence transcription in cis to DNA double-strand breaks. Cell *141*, 970–981.

Shimazaki, N., Tsai, A.G., and Lieber, M.R. (2009). H3K4me3 stimulates the V(D)J RAG complex for both nicking and hairpinning in trans in addition to tethering in cis: implications for translocations. Mol. Cell *34*, 535–544.

Simonis, M., Klous, P., Splinter, E., Moshkin, Y., Willemsen, R., de Wit, E., van Steensel, B., and de Laat, W. (2006). Nuclear organization of active and inactive chromatin domains uncovered by chromosome conformation capture-on-chip (4C). Nat. Genet. *38*, 1348–1354.

Skok, J.A., Gisler, R., Novatchkova, M., Farmer, D., de Laat, W., and Busslinger, M. (2007). Reversible contraction by looping of the Tcra and Tcrb loci in rearranging thymocytes. Nat. Immunol. *8*, 378–387.

Splinter, E., de Wit, E., Nora, E.P., Klous, P., van de Werken, H.J., Zhu, Y., Kaaij, L.J., van Ijcken, W., Gribnau, J., Heard, E., and de Laat, W. (2011). The inactive X chromosome adopts a unique three-dimensional conformation that is dependent on Xist RNA. Genes Dev. *25*, 1371–1383.

Su, R.C., Brown, K.E., Saaber, S., Fisher, A.G., Merkenschlager, M., and Smale, S.T. (2004). Dynamic assembly of silent chromatin during thymocyte maturation. Nat. Genet. *36*, 502–506.

Ward, I.M., Minn, K., van Deursen, J., and Chen, J. (2003). p53 Binding protein 53BP1 is required for DNA damage responses and tumor suppression in mice. Mol. Cell. Biol. *23*, 2556–2563.

Zha, S., Bassing, C.H., Sanda, T., Brush, J.W., Patel, H., Goff, P.H., Murphy, M.M., Tepsuporn, S., Gatti, R.A., Look, A.T., and Alt, F.W. (2010). ATM-deficient thymic lymphoma is associated with aberrant tcrd rearrangement and gene amplification. J. Exp. Med. *207*, 1369–1380.